The Relaxation Dynamics and Short-Time Optical Response of a Multimode Open System

Lowell W. Ungar[†]

Department of Chemistry, University of Utah, Salt Lake City, Utah 84112

Jeffrey A. Cina*[,†]

Department of Chemistry and Oregon Center for Optics, University of Oregon, Eugene, Oregon 97403

Received: March 24, 1998; In Final Form: July 8, 1998

When dividing a large system into a subsystem and a bath, one sometimes needs to include multiple nuclear coordinates in the subsystem in order to treat the remaining bath modes by Markovian relaxation theory (which assumes fast bath relaxation). This paper examines the effects of Redfield relaxation on the time-resolved fluorescence signal and on the loss of energy from a three-mode system. Simulations are compared for system coordinates coupled to the same bath mode and to independent bath modes, for coupling linear and quadratic in the system coordinates, and for different temperatures. To make these comparisons meaningful, a criterion is proposed for normalization of the coupling strengths in the different cases. The fluorescence Stokes shift and the system energy are shown to be sensitive to different relaxation processes. The coupling of multiple system coordinates to the same bath mode results in a wide range of relaxation rates. Simple descriptions in terms of individual population relaxation and coherence dephasing rates are inadequate due to sequential processes and to coupling between populations and coherences. These results have implications not only for Redfield treatments but also for other relaxation theories such as the Brownian oscillator model.

I. Introduction

Recent progress in the capability of femtosecond laser sources has fostered widespread investigation of chemical dynamics in condensed phases using a variety of time-resolved nonlinear optical measurements. In the most general (and vaguest) terms, these experiments optically excite a chromophore and measure the influence of interactions between the chromophore and a solvent on its subsequent evolution. The evolution can include both oscillatory coherent nuclear motion and incoherent population decay. Electron transfer and energy transfer also can cause vibrational coherences that are observable by ultrafast optical measurements.

If the temperature is sufficiently high compared to the relevant frequencies of nuclear motion and if the Born−Oppenheimer approximation holds, classical nonequilibrium molecular dynamics simulations can model the time evolution of the large numbers of solvent molecules responding to and influencing the excited chromophore. But often, some important features of the motion must be described quantum mechanically. Unfortunately, the rapid rise in the required number of basis functions with increasing degrees of freedom precludes incorporation of all solvent motions in a fully quantal treatment. Thus, approximate relaxation methods have been appropriated from magnetic resonance, quantum optics, and other areas of spectroscopy and dynamics. In this approach, a small number of modes are treated rigorously (the system) and the remainder are subsumed into a less carefully described bath.

The system typically comprises a bare minimum of important degrees of freedom, such as the optically coupled electronic levels subject to a resonant excitation, or the donor and acceptor states and a generalized collective nuclear coordinate in an electron-transfer reaction. While the most obvious decomposition recognizes the directly measured or excited degrees of freedom as the system and relegates everything else to the bath, other separations between system and bath may work better in some cases. In particular, solvent modes that are strongly coupled to the key coordinates may have to be included in the system.

Redfield theory[1,2] is one such approach to incorporating relaxation in a quantum dynamics calculation. In Redfield relaxation, the system evolves in contact with a bath that starts and stays in thermal equilibrium; the bath is unperturbed by the presence of the system and carries no memory of past states of the system. Often, however, an optically excited chromophore launches nonequilibrium dynamics in the surrounding medium. For example, in classical simulations of the cage effect in geminate recombination (in which the atoms in a photoexcited solute begin to dissociate impulsively but then collide with the surrounding solvent molecules) shock waves have been seen in the host medium.[3]

In principle, bath dynamics can be incorporated by going beyond the Markovian (memoryless) assumptions of Redfield theory. The theory becomes difficult in practice, but progress has been made along this line for some well-defined model problems.[4−9] Mixed quantum-classical methods have been employed as well, including some physically motivated but phenomenological approaches to the inclusion of quantum mechanical coherence loss.[10−12] Here, we explore a less demanding alternative approach; we retain the Markovian structure of Redfield theory and simply enlarge the "system" to include multiple nuclear degrees of freedom that couple strongly to an optically driven electronic transition but are not themselves directly excited by the external laser field.

[†] Some of this work was performed while the authors were at the Department of Chemistry and The James Franck Institute of The University of Chicago. J.A.C's e-mail address is cina@oregon.uoregon.edu.

S1089-5639(98)01600-4 CCC: $15.00
Published on Web 08/29/1998

As a simple nonlinear optical measurement in which to explore this approach, we choose the time-dependent Stokes shift of a "solvated" chromophore. Specifically, we simulate the peak frequency of the time-dependent fluorescence spectrum following short-pulse excitation, $\omega_{peak}(t)$. Under favorable circumstances, this quantity reflects the time-dependent average electronic transition energy $\Delta E(t)$, the expectation value of the potential difference between ground and excited electronic states as the nuclear distribution initially corresponding to ground-state equilibrium evolves in the excited electronic state. As time-resolved fluorescence is (in theory) one of the simplest nonlinear optical measurements and since excitation of the solute molecule induces nonequilibrium motion of nearby solvent molecules, the Stokes shift forms an ideal testing ground for our implementation of relaxation theory.

In this study, our system is a three-mode model whose simulated time-dependent fluorescence spectra have been exhaustively investigated.[13] The model system, a polar solute interacting with several polar solvent molecules, is here augmented with a surrounding medium that induces "vibrational" relaxation and dephasing in the system coordinates (the system coordinates are in fact librations). As our purpose is simply to make a preliminary test of relaxation theory in a multimode system and to explore different system−bath coupling schemes, we characterize the bath in only the most cursory terms and do not attempt to identify our model with any specific bulk polar solution.[14]

The simulated signals shown below are oscillatory and do not look much like the overdamped solvation Stokes shift experimental signals. Indeed, as a weak coupling theory, Redfield relaxation is only good for underdamped motion. However, small systems with Redfield relaxation similar to the one simulated here could model related experiments, such as the pump−probe spectroscopy of polyatomic chromophores in solution, of solutions with local solvent modes including cryogenic rare gas matrixes, and of chromophores in biological systems. In addition, solvation Stokes shifts and other overdamped signals could be due to "unphasing" of several modes, each of which is underdamped. With a few more system coordinates (and somewhat faster computers), one could simulate such overdamped signals using Redfield relaxation.

We address several issues of general importance in the application of relaxation theory to nonlinear optical signals. Can the probed quantity (in this case $\omega_{peak}(t)$) distinguish between different forms of system−bath coupling, e.g., coupling that is linear versus quadratic in the system coordinates and correlated versus uncorrelated among different system coordinates? What is the relative influence on the signal of vibrational energy relaxation and vibrational dephasing? Is the fluorescence Stokes shift an accurate probe of system energy relaxation? Are there relaxation phenomena specific to multimode systems? Do "nonsecular" relaxation processes, which couple system density matrix elements that oscillate at different frequencies, affect the signal?

An interesting technical issue arises in the comparison of different forms of the system−bath coupling. In an attempt to determine whether different system−bath couplings give rise to sensibly different optical signals, we must not misconstrue sensitivity to changes in coupling strength as an indication of sensitivity to different forms of system−bath interaction. To prevent this, we devise a normalization criterion whereby different forms of interaction may be said to have more-or-less equivalent interaction strengths.

The rest of the paper is laid out as follows. We first briefly describe our application of Redfield relaxation theory, the coupling normalization criterion, the simulated optical signal, and the model system. $\omega_{peak}(t)$ is then computed for different system−bath coupling schemes. Results with correlated and uncorrelated coupling are compared. In the context of correlated coupling only, quadratic and linear coupling are compared, the effects of linear-quadratic crossterms are examined, and the temperature dependence is discussed. We conclude with a brief extension of our discussion to the useful but phenomenological Brownian oscillator model and with some suggestions for future developments.

II. Methods and Model

II.A. Redfield Theory with a Simple Bath. Quantum dynamics simulations at present are possible with only a few degrees of freedom (except in some harmonic models). While few-mode models may be sufficient to simulate the initial motions of nearby solvent molecules in response to the electronic excitation of a chromophore, small systems do not allow effective dissipation of vibrational energy away from the chromophore, dephasing of coherent nuclear motion, or other effects of real baths. We will use Redfield theory[1,2,15] to include additional bath coordinates that are weakly coupled to the system. Under appropriate conditions, this approach can simulate relaxation of the small system, including both decay of vibrational coherences (dephasing) and vibrational population relaxation,[16] in a realistic manner.

We partition the full vibronic Hamiltonian into three parts:

$$\hat{H}_{tot} = \hat{H}_s + \hat{H}_b + \hat{V}(\mathbf{r},\mathbf{q}) \qquad (1)$$

a system Hamiltonian $\hat{H}_s$, a bath Hamiltonian $\hat{H}_b$, and a coupling $\hat{V}(\mathbf{r},\mathbf{q})$ that depends on both the system coordinates ($\mathbf{r}$) and a subset of bath coordinates coupled to the system ($\mathbf{q}$). The system includes key collective solvent coordinates and would include Franck−Condon active modes of the chromophore (fixed in our model).

The derivation of Redfield theory relies on the following assumptions.

(1) The system and bath density operators are initially separable, $\rho_{tot}(0) = \rho_s(0)\,\rho_b$. The density operator prepared by the excitation pulse will be separable if the system−bath coupling is negligible at equilibrium in the ground electronic state and in the propagation during the pulse and if the bath is affected by neither the pulse nor the electronic state.

(2) The coupling between the system and bath during the propagation is weak. In addition, the bath average of the coupling is assumed to be zero, $Tr_b[\rho_b\hat{V}(\mathbf{r},\mathbf{q})] \equiv \langle\hat{V}(\mathbf{r},\mathbf{q})\rangle = 0$, for any value of the system coordinate $\mathbf{r}$; the system Hamiltonian is then $\hat{H}_s = \langle\hat{H}_{tot} - \hat{H}_b\rangle$.

(3) Decay of the relevant bath correlation functions is rapid compared to the relaxation rates of the system (to enable a Markovian approximation).

Under the first two assumptions the Hamiltonian for a system that evolves adiabatically in the excited electronic state is

$$\hat{H}_{tot} = |g\rangle H_g\langle g| + |e\rangle H_e\langle e| + H_b + |e\rangle V(\mathbf{r},\mathbf{q})\langle e| \qquad (2)$$

where "g" and "e" refer to the ground and excited electronic states. H_g is used only for the initial density matrix following the excitation pulse and for the fluorescence, as the fluorescence signal reflects dynamics only in the excited electronic state.

The partition of a bulk solution into system and bath may not be simple. By assumption, the bath potential is not changed

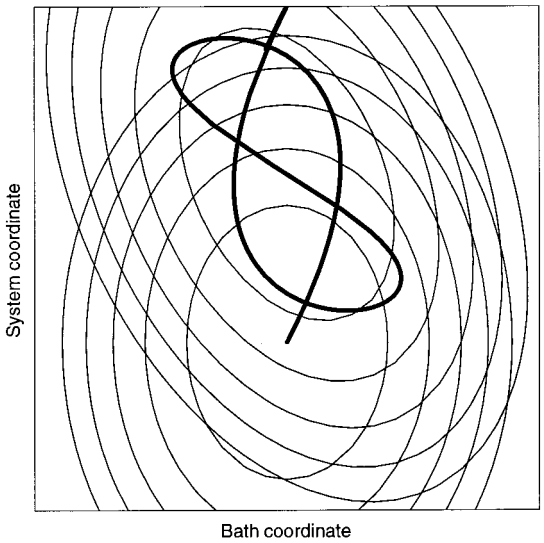

Figure 1. Illustration of motion induced in "bath" modes by excitation of the system. Contour plots are shown of a ground electronic state potential energy surface with one system and one bath mode and of a rotated and displaced excited-state potential. The heavier line shows the classical trajectory in the excited state starting at the minimum of the ground state. Although the potentials are displaced only in the system mode, motion is induced in the bath mode as well.

or displaced by the electronic state (although small changes could be incorporated in the system−bath coupling). However, the bath still can move following optical excitation; as illustrated in Figure 1, after the electronic state change displaces the system potential, coupling of the bath to the system nuclear coordinates displaces the bath equilibrium and causes bath motion. For the Markovian approximation to hold, the induced bath motion must be damped faster than the system relaxes. The assumptions of Redfield theory could be met by including in the subsystem a sufficiently large buffer of solvent coordinates between the excited chromophore and the bath, thus ensuring little disturbance of the bath. There is no guarantee, however, that such a subsystem could be defined small enough to enable rigorous treatment of its internal dynamics. In particular, we do not attempt to validate the assumptions for a small system in the polar solutions used in Stokes shift experiments. But these assumptions make feasible the simulation of the dissipative dynamics of a multimode system.

Under these conditions the effects of coupling to a bath on the evolution of the reduced system density matrix can be incorporated (using perturbation or projection operator techniques) in the Redfield relaxation tensor $R_{jk,lm}$,

$$\rho_{jk}(t) = -i\omega_{jk}\rho_{jk}(t) + \sum_{l,m} R_{jk,lm}\rho_{lm}(t) \tag{3}$$

where j, k, l, and m indicate nuclear eigenstates of the system, ρ is the system density matrix, ω_{jk} is the Bohr frequency $(\epsilon_j - \epsilon_k)/\hbar$, and A_{jk} is the element $\langle j|A|k\rangle$ of operator A. Pollard and Friesner[17] have shown that for system−bath coupling written as a sum of products of system and bath operators,

$$V(\mathbf{r},\mathbf{q}) = \sum_{a} G_a(\mathbf{r})F_a(\mathbf{q}) \tag{4}$$

the equations of motion can be written

$$\dot{\rho}_{jk}(t) = -i\omega_{jk}\rho_{jk}(t) + \frac{1}{\hbar^2}\sum_{a}\{[G_a^+\rho(t), G_a] + \text{h.c.}\}_{jk} \tag{5}$$

with

$$(G_a^+)_{jk} = \sum_{b} (G_b)_{jk}(\theta_{ab}^+)\omega_{jk} \tag{6}$$

$$(\theta_{ab}^+)_\omega = \int_0^\infty d\tau\, e^{-i\omega\tau}\langle F_a(\tau)F_b\rangle \tag{7}$$

Here h.c. is the Hermitian conjugate and $\langle F_a(\tau)F_b\rangle$ is a bath correlation function (with both equilibrium and evolution determined by H_b). The relevant bath dynamics are specified by $(\theta_{ab}^+)_\omega$ evaluated at the system Bohr frequencies ω_{jk}. As Pollard and Friesner have explained,[17] there is a computational advantage to evaluating $\dot{\rho}_{jk}(t)$ using eq 5 rather than eq 3. While the latter requires storage and multiplication of the N^4 Redfield tensor elements (where N is the number of system eigenstates), the former entails storing and multiplying only $N \times N$ matrixes, which scales as N^3.[18]

The system−bath coupling can be put in the form of eq 4 by expanding the coupling potential in terms of the displacements of the system and bath coordinates from an appropriate reference configuration $(\mathbf{r}_e,0)$ (the reference values of the bath coordinates q_a are arbitrarily set to zero).[19] To keep the displacements small at long times, the reference configuration should be near the average coordinates in the uncoupled Hamiltonians H_e and H_b. We choose $\mathbf{r}_e$ to be the lowest minimum of the system potential (slightly different from the average in our anharmonic system) so that the expansion does not depend on the temperature. For a harmonic system, pure dephasing enters only with coupling quadratic in the system coordinates; thus, to include appropriate dephasing for a system that is close to harmonic, we include coupling terms linear in the bath coordinates and up to quadratic in the system coordinates

$$V(\mathbf{r},\mathbf{q}) \approx \sum_{a}\left[\sum_{i}\frac{\partial^2 V(\mathbf{r}_e,0)}{\partial r_i\,\partial q_a}(r_i - r_{e,i}) + \frac{1}{2}\sum_{i,j}\frac{\partial^3 V(\mathbf{r}_e,0)}{\partial r_i\,\partial r_j\,\partial q_a}(r_i - r_{e,i})(r_j - r_{e,j})\right]q_a \tag{8}$$

In this approximation, the coupling operators in eq 4 are specified; $F_a = q_a$, and G_a is equal to the quantity in square brackets in eq 8. As $\langle V\rangle = 0$, terms zeroth order in the bath modes are incorporated in H_e. We assume there are no terms zeroth order in the system coordinates; such terms would incorporate differences between the bath potentials in the excited and ground electronic states (since H_b is the same in the two states, any difference must be included in the coupling). Coupling to many bath molecules can be included in relatively few explicit coordinates if q_a (and possibly r_i) represent collective motions of many molecules.

In principle, the derivatives of the coupling potential in eq 8 could be calculated from an analytical potential, and the bath correlation functions of eq 7 could be simulated using classical molecular dynamics[20,21] or derived from experiment.[22] Instead, we will posit a bath that allows realistic dissipation while inherently obeying the assumptions of Redfield theory. The coupling derivatives are treated as parameters. We make some dramatic assumptions to simplify the relevant bath dynamics, being careful to preserve detailed balance.[19,23] We neglect entirely the imaginary parts of θ^+, allowing the correlation function in eq 7 to be symmetrized. The bath coordinates are assumed to be linearly independent, $\langle q_a(\tau)q_b\rangle = 0$ for $a \neq b$ (but one bath coordinate may be coupled to multiple system

coordinates; see section III.B). Extending the Redfield approximation of fast relaxation of the bath, the symmetrized correlation functions are assumed to decay quickly compared to the nuclear Bohr frequencies of the system. If the fast decay of the correlation functions is exponential, $(1/2)\langle q_a(t)q_a + q_aq_a(t)\rangle = \langle {q_a}^2\rangle \exp(-|t|/\tau_a)$, then

$$(\theta^+_{ab})_\omega = \delta_{a,b}\frac{1}{1+e^{\beta\hbar\omega}}\int_{-\infty}^{\infty} d\tau\, e^{-i\omega\tau}\frac{1}{2}\langle q_a(\tau)q_a + q_aq_a(\tau)\rangle \approx \delta_{a,b}2\tau_a\langle q_a^2\rangle\frac{1}{1+e^{\beta\hbar\omega}} \quad (9)$$

($\beta = 1/k_bT$). The frequency dependence of $(\theta^+{}_{ab})_\omega$ maintains detailed balance. The prefactor $2\tau_a\langle q_a^2\rangle$ also is treated as a parameter; it is redundant with the coupling derivatives and need not be separately specified. Note from the first equality in eq 9 that with these assumptions $(\theta^+{}_{ab})_\omega$ is closely related to the spectral density of the system−bath coupling.

II.B. Normalization of Different System−Bath Couplings. To fairly compare the effects of different ways of coupling the bath to the system, we need to "normalize" the overall rate of dissipation in each case. Our criterion will be the rate at which energy is absorbed by the bath under the influence of the evolving system. Specifically, two forms of coupling to a bath are considered normalized if the associated baths absorb energy at equal rates from the system when the system evolves without feedback from the bath. The rates are averaged over a time that is long compared to the system periods. In this hypothetical situation, considered solely for the purpose of normalization, the system acts as an oscillating force on the bath due to its coherent motion. The force that acts on the bath coordinate $q_a = F_a$ is taken to be $-\langle G_a(t)\rangle_s$, the time-dependent average of $-G_a(\mathbf{r})$ under the evolving distribution of the isolated system. When expanded in the system eigenstates, $\langle G_a(t)\rangle_s$ is a sum of discrete-frequency components

$$\langle G_a(t)\rangle_s = Tr[\exp(-iH_et/\hbar)\rho(0)\exp(iH_et/\hbar)G_a(\mathbf{r})] = \sum_{j,k}\rho_{kj}(0)(G_a)_{jk}\exp(-i\omega_{kj}t) \quad (10)$$

The initial density operator, $\rho(0)$, is set identical to the thermal equilibrium density operator (see section II.C) transferred unchanged to the excited electronic state so that the normalized coupling will not depend on the laser pulses.

Assuming that none of the Bohr frequencies are degenerate, the time-averaged rate of energy absorption into independent bath coordinates q_a is[24]

$$\dot{E}_{bath} = \sum_{a,j,k}\omega_{jk}\alpha_a''(\omega_{jk})|\rho_{kj}(0)(G_a)_{jk}|^2 \quad (11)$$

where $\alpha_a''(\omega)$ is the imaginary part of the frequency-dependent susceptibility associated with bath mode q_a. If the force on q_a from the system is weak (as it must be for Redfield theory to be valid), the fluctuation−dissipation theorem shows that $\alpha_a''(\omega)$ is proportional to the real part of $(\theta^+{}_{aa})_{-\omega}$[24] and hence can be evaluated using the same assumptions (listed above eq 9):

$$\alpha_a''(\omega) = \frac{1}{\hbar}\tanh\left(\frac{\beta\hbar\omega}{2}\right)\int_{-\infty}^{\infty} d\tau\, e^{i\omega\tau}\frac{1}{2}\langle q_a(t)q_a + q_aq_a(t)\rangle \approx \frac{2\tau_a\langle q_a^2\rangle}{\hbar}\tanh\left(\frac{\beta\hbar\omega}{2}\right) \quad (12)$$

Thus, the final expression for the hypothetical rate of energy loss to the bath in the absence of feedback to the system is

$$\dot{E}_{bath} = 2\sum_{\substack{a\\k>j}}\frac{2\tau_a\langle q_a^2\rangle}{\hbar}\left(\frac{\beta\hbar\omega_{kj}}{2}\right)\omega_{kj}|\rho_{kj}(0)(G_a)_{jk}|^2 \quad (13)$$

Note that in this expression the bath absorbs energy only under the influence of system coherences, as the Bohr frequency of the populations, ω_{jj}, is zero. For example, incoherent distributions among eigenstates will dissipate no energy in this normalization calculation because they do not move in an isolated system. Thus, the normalization reflects absorption by the bath only of energy from coherent motion in the system, while the decay of the system energy in actual simulations also includes incoherent population relaxation of a nonthermal distribution.

II.C. Calculation of the Fluorescence Signal. The observable that will be simulated is the peak frequency of the time-dependent fluorescence spectrum following excitation by a short pulse as observed by fluorescence upconversion. We previously derived an expression for this observable and examined it for our model system;[13,25] here we just give the expression (equivalent to eqs B1−B3, the "observed" spectrum, in ref 13). The initial density matrix $\rho(0)$ is a piece of the ground electronic state equilibrium density matrix promoted to the excited state by a short pulse:

$$\rho(0) = P(\Omega_{exc},\tau_{exc})\rho_{eq}P^\dagger(\Omega_{exc},\tau_{exc}) \quad (14)$$

where $\rho_{eq} = \exp(-\beta H_g)/\mathrm{Tr}[\exp(-\beta H_g)]$, and

$$P(\Omega_p,\tau_p) = -\frac{i}{\sqrt{2\pi}\tau_p}\int_{-\infty}^{\infty} d\tau\exp(-\tau^2/2\tau_p^2)\times \exp[i(H_e-\hbar\Omega_p)\tau/\hbar]\exp(-iH_g\tau/\hbar) \quad (15)$$

is the pulse propagator for electronic excitation by an optical pulse with center frequency Ω_p and duration τ_p. After the pulse action, the density matrix is propagated in the excited state as described in section II.A. Assuming that the excitation pulse and upconversion pulse are separated in time, the time-dependent fluorescence spectrum observed by upconversion is a window on the propagated density matrix component

$$F(\omega,t_d) = \mathrm{Tr}[P(\omega,\tau_{up})P^\dagger(\omega,\tau_{up})\,\rho(t_d)] \quad (16)$$

This expression is equivalent to the stimulated-emission component of a pump−probe signal under similar conditions.[13] The peak fluorescence frequency at a given time, $\omega_{peak}(t_d)$, can be found from the maximum of the signal $F(\omega, t_d)$ with respect to frequency ω (noting that ω occurs only in the upconversion pulse propagators).

In calculating the time-resolved fluorescence spectrum $F(\omega, t_d)$ for a system and bath, we include relaxation via the Redfield tensor during the evolution in the excited state between the temporal centers of the excitation and upconversion pulses, but we neglect relaxation in calculating the pulse propagators (as well as neglecting effects of pulse overlap).[26] All simulations in this paper use an excitation pulse length of 10 fs and an upconversion pulse length of 20 fs. The excitation pulse center frequency is resonant with the vertical electronic transition of the system (defined as zero).

The density matrix was propagated in the interaction representation (with the system Hamiltonian H_e as the zeroth-order Hamiltonian) using Runge−Kutta integration.[27] A total of 269

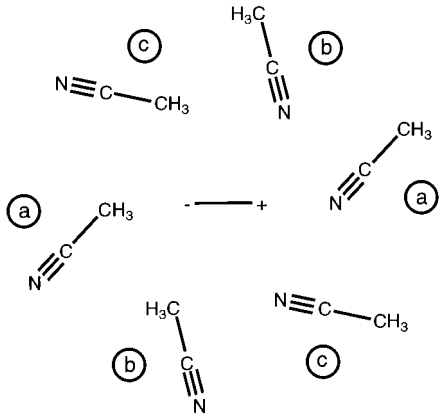

Figure 2. Geometry of the model system. Six acetonitrile molecules librate about fixed centers in a plane and respond to a change, upon electronic excitation, in the dipole moment of a diatomic "solute". The "solvent" orientations shown correspond to the equilibrium configuration in the electronic ground state. The labeled pairs are constrained to librate in tandem, reducing the number of degrees of freedom to three.

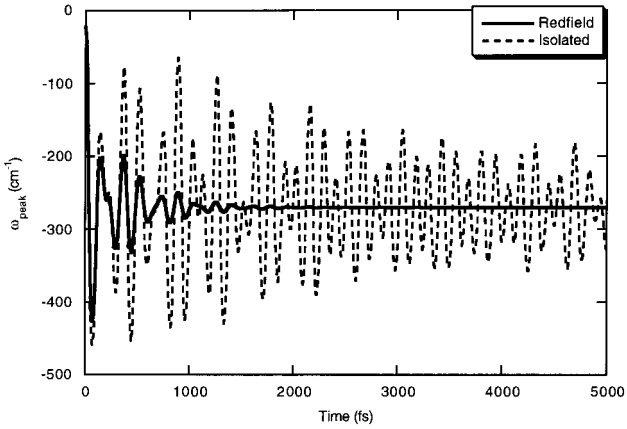

Figure 3. Peak frequency of the time-dependent fluorescence spectrum with inclusion of relaxation via Redfield theory. The three-coordinate system, the system−bath coupling, and the pulses are described in the text. Results are shown for uncorrelated system−bath coupling, with each of the three system coordinates coupled to an independent bath coordinate (—). Also included is the peak fluorescence frequency for an isolated system (- - -).

states in the ground manifold and 240 states in the excited manifold were included, but during the propagation high-lying states with small populations ($<10^{-5}$) were dropped from the calculation.

II.D. Model System. The system models a few key coordinates of a polar solvent around a polar solute. It also has been fully described in a previous paper,[13] but the most important points will be reiterated here. As illustrated in Figure 2, the model has three degrees of freedom with motions reminiscent of librations in the first solvation shell of acetonitrile, which have been shown to dominate the initial Stokes shift evolution.[28] Six CH_3CN molecules are arrayed in a plane around a fixed diatomic "solute", with fixed centers of mass 4.0 Å from the center of the solute and from each other. The coordinates are the in-plane rotations of these "solvent" molecules around their centers of mass; the number of dynamical degrees of freedom is reduced from six to three by artificially constraining pairs of CH_3CN molecules on opposite sides of the solute to rotate in tandem.

The united atoms interact via Lennard−Jones and Coulombic potentials with parameters taken from Edwards et al.[29] The solute is intended roughly to resemble a dipolar dye molecule; its two sites are split by 2.0 Å and have opposite charge. The only difference between ground and excited electronic states is a change in charge of the two solute sites from $\pm 0.6e$ to $\pm 1.0e$, changing the dipole moment from 5.76 to 9.61 D. Unless otherwise specified, calculations assume room temperature (300 K).

Several characteristics of the system can be extracted from the potential. The frequencies of the normal modes at the ground-state potential minimum are 194, 252, and 264 cm^{-1}, and those of the excited state at its minimum are 188, 265, and 296 cm^{-1} (we will refer to the excited-state modes as 1, 2, and 3, respectively). The molecular librations are highly mixed in the normal modes. The difference in the excited-state potential energy between the configurations for the lowest ground-state minimum and lowest excited-state minimum (roughly the solvation energy) is -174 cm^{-1}. The change in difference potential between these two configurations (roughly the steady-state Stokes shift) is -343 cm^{-1}. The orientational displacement upon excitation is small, especially in the libration labeled 'b'. In terms of the excited-state modes, the displacements are 0.928, -0.767, and $0.366\sqrt{\hbar/m_i\omega_i}$ for modes 1, 2, and 3. Although there are several wells in each state, only one is significant at room temperature and needs to be included in the calculations.

III. Simulation Results and Comparison of Different System−Bath Interactions

III.A. Redfield Relaxation. The time-dependent peak fluorescence frequency from the photoexcited model system with coupling to a Redfield bath is shown in Figure 3. The peak fluorescence frequency from the isolated system is shown for comparison. For this plot, the three system coordinates—the molecular librations, not the normal modes—are each coupled to an independent bath mode (uncorrelated or independent coupling). The strength of coupling, linear and quadratic, in the system coordinates (and the magnitudes and relaxation times of the bath coordinate fluctuations) are chosen to be the same for each mode

$$V_{\mathrm{ind}}(\mathbf{r},\mathbf{q}) = \sum_i [G'_{\mathrm{ind}}(r_i - r_{e,i}) + G''_{\mathrm{ind}}(r_i - r_{e,i})^2]q_i \qquad (17)$$

The ratio of quadratic to linear coupling, G''/G', is set to 8 rad^{-1}, a value chosen so that both linear and quadratic coupling have a significant effect on the fluorescence signal. The overall coupling strength is normalized as described in section II.B such that the bath would absorb energy at a rate of 30 cm^{-1}/ps from undamped system motion. The actual energy dissipation rate from the damped system in simulations at 300 K is almost an order of magnitude larger; this difference will be discussed in section III.B.

In Figure 3, the signal from the open system decays much faster than the comparison signal from the isolated system. At short times, there is considerable smoothing of the signal, with missing small features, but the oscillation frequencies appear unchanged. At longer times, the small residual signal oscillation (barely visible in the figure from 1.5 to 2.5 ps) is very different from the undamped signal. Its dominant oscillation is at the frequency of mode 1 (188 cm^{-1}), while the most prominent oscillation in the undamped signal is of mode 2 (265 cm^{-1}).

As mentioned in the Introduction, the simulated signal is very similar to the time-dependent average of the potential difference

TABLE 1: Comparison of the Redfield Tensor Elements for Different Forms of the System−Bath Coupling[a]

coupling	G'	G''/G'	$\dot{E}_{bath}$	$R_{00,11}$	$R_{01,01}$	$R_{00,22}$	$R_{02,02}$	$R_{00,33}$	$R_{03,03}$
uncorrelated	1.14	8	30	6.19	−10.08	5.08	−9.51	4.74	−9.16
correlated	1	8	30	13.54	−15.66	0.52	−6.97	0.00	−6.57
linear	1.06	0	30	14.13	−15.94	0.58	−6.40	0.00	−6.01
quadratic	5.21	∞	30	0.45	−16.48	0.00	−10.80	0.00	−9.52
crossterms	1.08	−8	30	13.64	−16.32	0.59	−6.11	0.00	−5.66
low-temp	1	8	442	19.08	−9.79	0.67	−0.89	0.00	−0.50

[a] All the couplings except the first are "correlated". The couplings are normalized as described in section II.B. The lowest tensor elements representing population relaxation ($R_{jj,kk}$) and dephasing ($R_{jk,jk}$) are given, roughly corresponding to a single excitation in each of the three system normal modes. G' (G'' for quadratic coupling) values are relative values of the parameters; the other units are rad^{-1} for G''/G', cm^{-1}/ps for $\dot{E}_{bath}$, and ps^{-1} for the tensor elements. See section III for description of the different coupling forms.

between the electronic states, $\Delta V = H_e - H_g$,

$$\omega_{peak}(t) \approx \Delta E(t) = \sum_{j,k} \rho_{jk}(t)\langle j|\Delta V|k\rangle \qquad (18)$$

The oscillations in $\Delta E(t)$ and in $\omega_{peak}(t)$ mostly reflect coherent motion of the system, manifested in the oscillations of the system coherences. In the isolated system, the contributions of mode 1 to $\omega_{peak}(t)$ decay faster than those of mode 2 because mode 1 has a broader range of frequencies (due to anharmonicity). But interaction with the bath causes both modes to dephase faster with roughly the same rate, leaving a slightly larger oscillation in mode 1 due to the slightly larger displacement in that mode. Mode 3 is somewhat less important in both cases because there is a smaller displacement from the ground state and thus smaller coherences, ρ_{jk}, and smaller matrix elements of ΔV.

The rates of both librational population relaxation and dephasing are determined by the elements of the Redfield tensor $R_{jk,lm}$. Of particular note are the elements $R_{jj,kk}$, each of which gives the population decay rate from state k to state j (there also is a smaller excitation rate $R_{kk,jj}$), and $R_{jk,jk}$, which gives a rate of dephasing of the coherence between states j and k independent of other density matrix elements. These tensor elements are given in Table 1 for the transitions between the ground librational state (0) and the first three excited states (1, 2, and 3), which each have one quantum in one mode (approximately, as the system is not exactly harmonic). All Redfield tensor elements other than $R_{jj,kk}$ and $R_{jk,jk}$ connect density matrix components that oscillate at different frequencies. If these relaxation terms (called "nonsecular") are small compared to the frequency mismatch, their impact will oscillate in time, averaging to zero. For the "uncorrelated" parameters used in Figure 3, the tensor elements between the lowest state and the first excited state in each mode range from 4.7 to 10.1 ps^{-1}. As illustrated by these examples, when system coordinates are coupled to independent bath modes, the three modes relax at rather similar rates.

However, as many tensor elements can contribute to Redfield relaxation, a single tensor element cannot be taken as a relaxation rate. Thus, the damping of the signal in Figure 3 is slower than the elements shown in Table 1 alone might suggest. The damping is slowed because relaxation processes are often sequential; e.g., the population in state 4 (doubly excited in mode 1) mostly transfers to state 1 and then to state 0. Coherences also can grow due to transfer from other coherences, such as ρ_{14} to ρ_{01}. The effect of such sequential processes is illustrated in Figure 4, in which the signal from a simulation that includes only the four lowest vibrational states is shown to decay much faster than the signal from the full system (in addition to the smaller initial amplitude of oscillation). In principle, relaxation between modes, such as that reflected in $R_{11,22}$ and $R_{01,02}$, could speed the relaxation of the some modes and slow relaxation of other modes. For this system, however, such rates are mostly negligible.

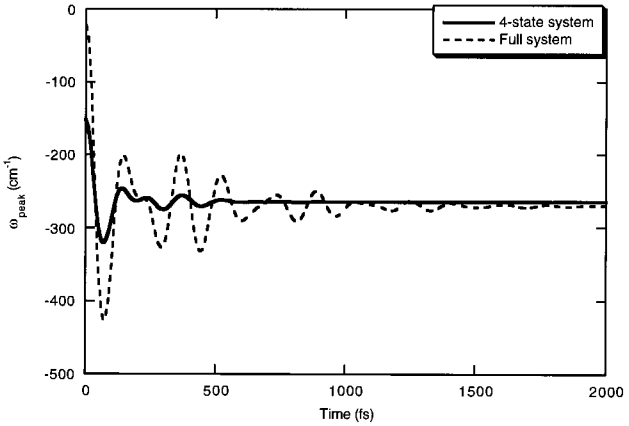

Figure 4. Peak frequency of the time-dependent fluorescence spectrum including only the first four states in the excited manifold compared to the signal from the full system. This demonstrates the importance of transfer between coherences.

III.B. Correlated and Independent Bath Coordinates. The signal with independent coupling is compared to the signal from a system in which all three coordinates are coupled to the same bath mode (correlated coupling) in Figure 5a. The form of the correlated system−bath coupling is

$$V_{corr}(\mathbf{r},q) = [G'_{corr}\sum_i (r_i - r_{e,i}) + G''_{corr}\sum_i (r_i - r_{e,i})^2]q \qquad (19)$$

Again the coupling strengths and bath relaxation times are chosen to be the same for all coordinates, $G''/G' = 8$ rad^{-1}, and the coupling strength is normalized so that $\dot{E}_{bath} = 30$ cm^{-1}/ps. The optical signals for these two cases are somewhat similar for about 600 fs. After that, a persistent oscillation in mode 2 dominates the signal with correlated coupling. Thus, the form of the signal is much different, and the decay is much slower than that in the signal with independent coupling. The slow damping of mode 2 is consistent with the Redfield tensor elements ($|R_{02,02}| < |R_{01,01}|$).

The decay of the system energy, shown in Figure 5b, depends even more strongly on the coupling form. The figure shows the actual time-dependent average system energy in the simulations, not to be confused with the hypothetical energy decay rate used in the normalization. The energy of the system coupled to independent bath modes decays much faster than the energy of the system coupled to a single bath mode but with a more prominent oscillation (corresponding to mode 1).

The system energy evolution is quite different from that of the optical signal because it depends on different system properties. While the signal is affected mostly by system coherences, the system energy at a given time depends only on

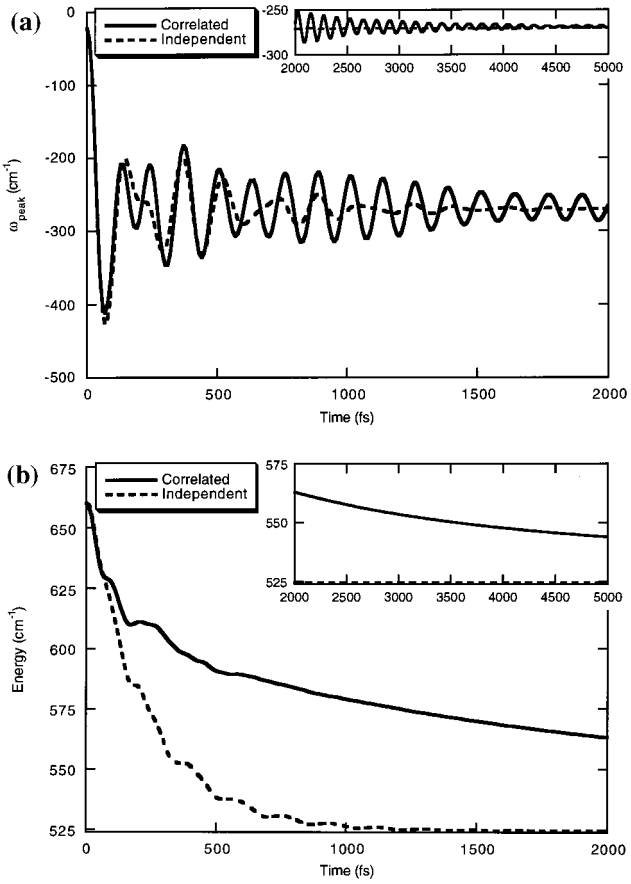

Figure 5. Comparison of coupling of the three system coordinates to the same (—) and to independent (- - -) bath coordinates. The system and the pulses are the same as those in Figure 3. Part a shows the peak fluorescence frequency, and part b shows the average system energy. The insets continue the figures to longer times (with a different horizontal scale).

the librational populations: $E = \sum_j \rho_{jj} \epsilon_j$. The signal tracks coherent motion of the system, but energy dissipation includes loss of incoherent or random thermal energy as well as damping of coherent motion. Experimentally, vibrational energy loss rates can sometimes be inferred from the time dependence of signal oscillations; the oscillations tend to speed up as the system relaxes to states lower in the potential well (especially in systems with larger Stokes shifts than ours has).[30] Time-resolved Raman spectroscopy can also probe thermal energy changes in a chosen vibration. Recent work by Iwata and Hamaguchi: [Iwata, K.; Hamaguchi, H. *J. Phys. Chem. A* **1997**, *101*, 632.] monitored the cooling of the C═C stretch in photoexcited S_1 *trans*-stilbene using such a "picosecond Raman thermometer" method.

The different energy dissipation rates in Figure 5b illustrate a significant difference between correlated and independent coupling. The initial dissipation rate in both cases is very fast, comparable, when divided by a characteristic librational energy, to the largest Redfield terms in Table 1 (not surprisingly). However, within 100 fs the system energies diverge sharply from each other. Some of the population relaxation rates that result from correlated coupling are considerably faster than those from uncorrelated coupling, and some are very slow. The $R_{jj,kk}$ terms with correlated coupling in Table 1 vary over 8 orders of magnitude, while the terms with independent coupling (and the $R_{jk,jk}$ dephasing terms) are all of the same order of magnitude. Hence, with correlated coupling, after most populations are in equilibrium with each other, a few populations continue to decay slowly and the energy only slowly reaches its thermal value.

The reason some population relaxation rates that result from correlated coupling are increased and some greatly suppressed is because multiple system coordinates are coupled to the same bath mode. The effects of the different system coordinates on the bath mode can enhance or cancel each other, manifesting in a constructive or destructive sum over system coordinates in the tensor element

$$R_{jj,kk} = (\theta^+)_{\omega_{jk}} \frac{2}{\hbar^2} [\sum_i G'_{\mathrm{corr}}(r_i - r_{e,i})_{jk} + G''_{\mathrm{corr}}((r_i - r_{e,i})^2)_{jk}]^2 \qquad (j \neq k) \quad (20)$$

Note that G'_{corr} was arbitrarily chosen to be the same for all system coordinates; different choices would cause different relaxation rates to be enhanced or suppressed. When the coupling is uncorrelated, this interference cannot happen; as the system coordinates are coupled to different modes, the tensor element is a sum of squares rather than a square of a sum. As is evident in Table 1, the same kind of interference can occur with purely linear or purely quadratic coupling. Such interference under correlated coupling also affects the damping of the optical signal, but the effect is less dramatic because many more terms contribute to the $R_{jk,jk}$ elements. Under the assumptions used here, $R_{jk,jk}$ can be written

$$R_{jk,jk} = -\tau\langle q^2\rangle \frac{1}{\hbar^2}(G_{\mathrm{corr},kk} - G_{\mathrm{corr},jj})^2 - \frac{1}{2}\sum_{m\neq j} R_{mm,jj} - \frac{1}{2}\sum_{m\neq k} R_{mm,kk} \quad (21)$$

where G_{corr} corresponds to the quantity in square brackets in eq 20. The interference is unlikely to affect all the terms at once.

The enhancement or suppression of dissipation due to constructive or destructive contributions among different system coordinates is an interesting example of a relaxation process specific to a multicoordinate system. Enhanced population relaxation (phonon emission, as from state 1) can be regarded as the material analogue of the enhanced light emission that occurs from multiple excited sources in the optical process of superradiance, and suppressed population relaxation (as from states 2 and 3) is the analogue of subradiance.[31]

A second reason for the relative similarity at early times of the optical signal decay rates with correlated and independent coupling is that it results from the normalization. The hypothetical dissipation that determines the normalization rate reflects energy emission to the bath via coherent motion but not dissipation of incoherent energy; the normalization rate is proportional to the square of the system vibrational coherences created by the excitation pulse but does not depend directly on the populations (see eq 13). Thus, the Stokes shift, which also depends mostly on system coherence, is fairly well normalized. But the larger portion of dissipation from this system is neglected by the normalization. Hence, the simulated dissipation rates are much greater than the hypothetical rate, and the simulated rates can vary.

Oscillations in the system energy are due to nonsecular transfers between populations and coherences. These couplings are an essential feature of realistic dissipation.[32] The prominent oscillation in the energy for independent system−bath coupling is due to a fairly large term between the ρ_{01} coherence and the ρ_{00} ground librational state population, $R_{00,01} = 1.96$ ps^{-1}.

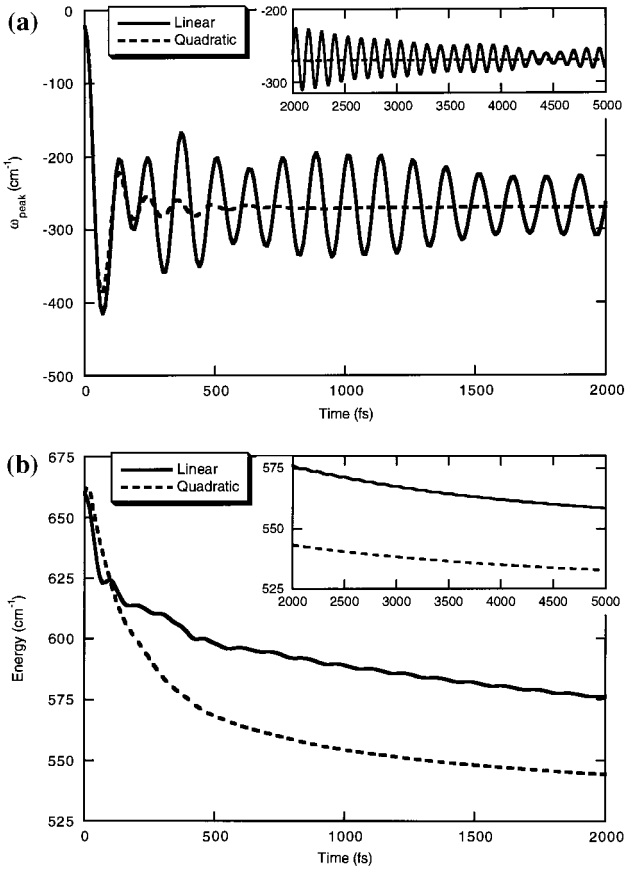

Figure 6. Comparison of the effects of correlated coupling, linear and quadratic, in the system coordinates. Peak fluorescence frequency for the pulses and system of Figure 3 with purely linear coupling (—) and purely quadratic coupling (- - -). Part a shows the peak fluorescence frequency, and part b shows the average system energy.

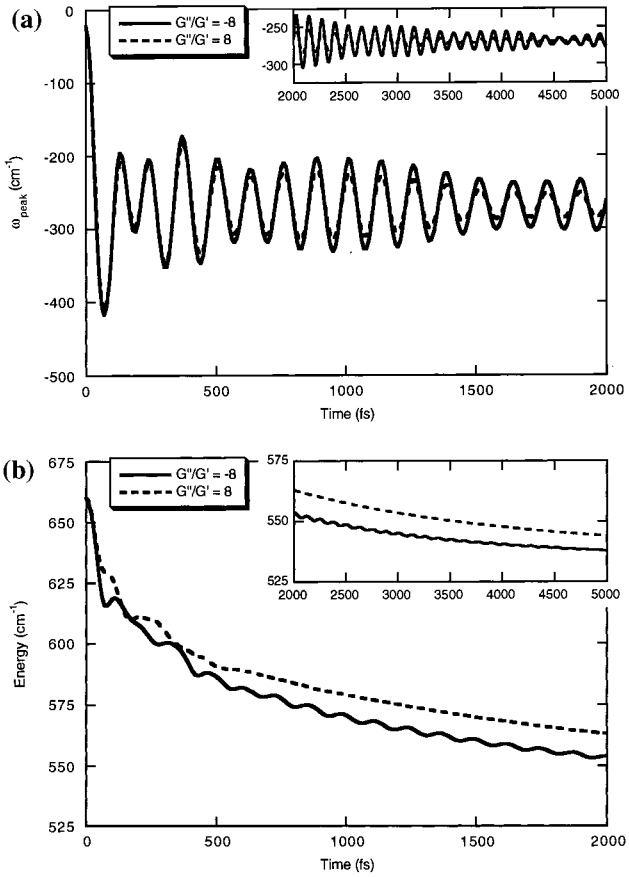

Figure 7. Demonstration of the importance of linear and quadratic crossterms. Comparison of the peak fluorescence frequency (a) and the average system energy (b) for the pulses and system of Figure 3, with $G''/G' = -8$ (—) and $G''/G' = 8$ (- - -).

Note also that with independent coupling, the signal oscillations are apparent well after the energy has decayed to very close to its equilibrium value. In this case, significant coherences remain after population relaxation is nearly complete, causing coherent motion in a system with nearly thermal populations. With correlated coupling, incoherent relaxation continues after the coherent motion has essentially disappeared (this is clearer with purely quadratic coupling, shown in Figure 6 parts a and b below).

III.C. Linear and Quadratic Coupling. The differences between relaxation with coupling, linear and quadratic, in the system coordinates are even more dramatic. In Figure 6a the signals with purely linear coupling and with purely quadratic coupling are compared for coupling to a single bath coordinate (again the subsystem and pulses are the same as in Figure 3). Both signals are normalized as described in section II.B. The quadratic coupling causes much faster decay in the oscillations of the fluorescence signal than does linear coupling. The difference between the effects of linear and quadratic coupling is simplest in harmonic systems, in which quadratic coupling causes pure dephasing but does not cause population relaxation between adjacent levels. As the system here is not highly excited, it is fairly close to harmonic. Since the fluorescence frequency is mostly determined by the average configuration of the system, with motion arising mostly from system librational coherences, the signal oscillations are effectively damped by pure dephasing due to quadratic coupling. Energy dissipation and the normalization, on the other hand, are primarily due to the elements of the coupling $G_a(\mathbf{r})$ that cause population relaxation between adjacent levels and therefore are sensitive to linear coupling. Because of the normalization, the quadratic coupling is relatively strong and the resultant optical signal decays very quickly. Although the dominant frequency is the same with linear and quadratic coupling, there is a small phase shift due most likely to the different damping rates.

The energy decay is well normalized for the first 100 fs (Figure 6b). Afterward, the energy with quadratic coupling decays more quickly than the energy with linear coupling even though the Redfield tensor population relaxation elements in Table 1 are much smaller. Although quadratic coupling does not couple adjacent states in a harmonic mode, it does couple states j with $j \pm 2$. The first excited state in each mode has no state $j - 2$ to couple to and thus decays slowly, but the normalized coupling between many of the higher-lying states is relatively strong and causes faster relaxation. The energy decay with quadratic coupling is very smooth because the coherences dephase so quickly. The energy oscillation with linear coupling reflects continued coherence in mode 2.

Comparison of the signals for $G''/G' = 8$ and -8 rad^{-1}, with different sign of the quadratic coupling relative to the linear coupling (both to a single bath mode), highlights the effects of the crossterms of linear and quadratic coupling in the Redfield tensor. For a harmonic system, these crossterms would couple populations to coherences and coherences to each other; all these terms in the Redfield tensor would be neglected under a secular approximation. The relative sign of the linear and quadratic coupling and hence their crossterms does have a small effect on the fluorescence signals and system energies in Figure 7. The signal oscillation in mode 2 is slightly less damped with $G''/G' = -8$. However, the energy decays somewhat faster.

The individual Redfield tensor elements, particularly the nonsecular terms, can differ in the two cases by a factor of 2 or more (though the terms in Table 1 are quite similar).

III.D. Temperature Dependence. The temperature dependence of the dissipation combines several different factors. At low temperature, the system is more coherent (the coherences between vibrational states in the electronically excited component of the density matrix are larger) because fewer vibrational states of the ground electronic manifold are populated in the initial thermal distribution. Fewer and lower states in the excited manifold are populated as well (both initially and at final equilibrium). Temperature also affects the frequency dependence of θ^+ and α'' through the temperature dependence of the bath correlation functions. Because of detailed balance, the magnitude of terms that cause downward transitions in the simulations and in the normalization increases with decreasing temperature (see eq 9 with $\omega < 0$ and eq 12); upward transitions are shut off. This effect is most pronounced for frequencies comparable to the temperature (208.5 cm^{-1} at room temperature). There is an additional temperature dependence: the bath fluctuations $\langle q_a^2 \rangle$ shrink with decreasing temperature. Since in Redfield theory the relaxation is proportional to the equilibrium fluctuations of the bath, this effect would decrease dissipation at low temperature. The size of this effect would depend on the exact nature of the bath, which we have avoided specifying. Thus, we neglect the temperature dependence of the bath fluctuations; as the temperature drops to become much smaller than the frequencies of bath modes resonant with system transitions, zero-point motion would make this dependence vanish anyway.

The signal with correlated coupling for a system and bath at 10 K is compared to the signal for system and bath at 300 K in Figure 8a. The coupling is *not* renormalized; the normalization−dissipation rate at 10 K is 442 cm^{-1}/ps. The normalization rate is strongly increased at low temperature, mostly because it is proportional to the squares of the larger coherences (see eq 13). Despite the greater initial coherence at low temperature, the peak frequency traces are quite similar. The width of the fluorescence spectrum (not shown) is narrower at low temperature. The signal at longer times (in the inset) is damped somewhat more slowly at 10 K. Damping is slower because dephasing of states low in the manifold is generally slowed at low temperature, as can be seen in Table 1. The dephasing of these states is slowed because population transfer to higher-energy states is shut off at low temperature; in eq 21 the $R_{mm,jj}$ and $R_{mm,kk}$ contributions with $m > j,k$ become small. The final values of the peak frequency are different because the average coordinates depend on temperature in this anharmonic system.

The energy dissipation at 10 K is compared to that at 300 K in Figure 8b. In each case, the energy is plotted relative to its value at thermal equilibrium. The initial superthermal energy is roughly the Franck−Condon energy in the excited electronic state and hence varies little with temperature. It is slightly lower at room temperature because of the finite excitation pulse duration.[33] At early times, energy dissipates more quickly from the low-temperature system despite the similarity of the superthermal energies. Interactions with a low-temperature bath are more likely to relax the system and less likely to excite it, reflected in larger population relaxation elements in Table 1 and smaller excitation elements at low temperature. But the excited populations are smaller at low temperature, slowing relaxation and counteracting the effect of the larger Redfield elements in eq 3. The net result for a linearly displaced harmonic oscillator (and energy relaxation is due primarily to linear coupling with the parameters used here) under the secular approximation is exponential decay of the superthermal energy at the rate: $\Gamma = \tau\langle q^2\rangle m^{-1}G'^2\langle H_e\rangle_e^{-1} = \tau\langle q^2\rangle m^{-1}G'^2 2(\hbar\omega)^{-1} \times \tanh(\beta\hbar\omega/2)$ (compare eqs 25, 50, and B8 in the second reference in ref 32); the inverse proportionality of the rate to the thermal energy $\langle H_e\rangle_e$ is similar to what is found in our simulation. After about 200 fs, the rate of energy loss slows, becoming slightly slower than that at 300 K. In both cases, after most populations reach equilibrium with each other, the rate of the remaining dissipation is limited by the slowest relaxation rates (recall that with correlated coupling there is a wide variety of population relaxation rates). The long-time dissipation rate will be somewhat temperature dependent because at low temperature the widely varying relaxation rates are averaged over fewer states.

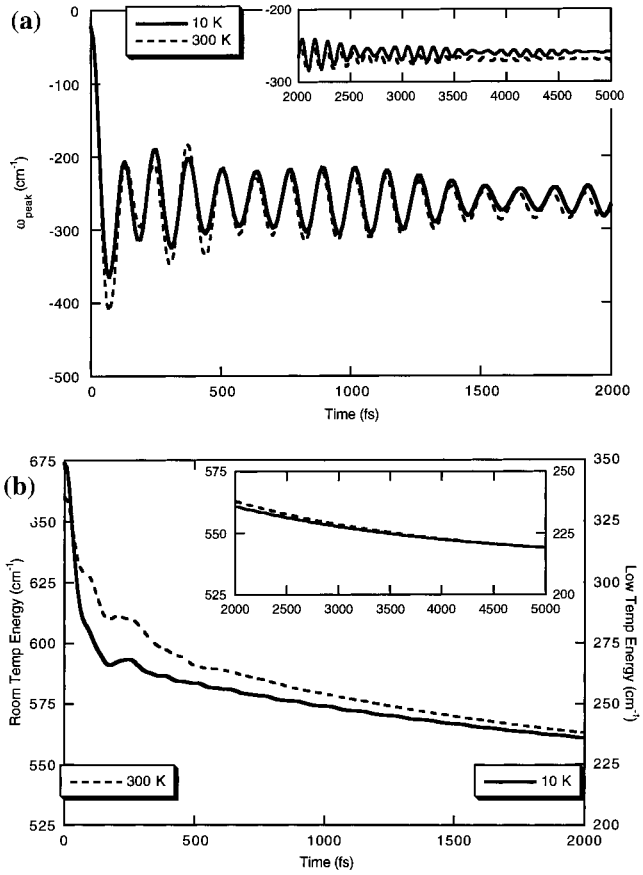

Figure 8. Effects of relaxation at low temperature. The peak fluorescence frequency (a) and system energy (b) for the system and bath at 10 K (—) are compared to the signal from the system at 300 K (- - -). Pulse parameters are the same as those in Figure 3. The temperature dependence of the bath fluctuation amplitude is neglected (see text). Note the shifted energy scales in Figure 8b—the bottom of the figure in each case is the thermal energy at that temperature.

IV. Concluding Remarks

Redfield and other relaxation theories are usually applied to either a single system coordinate (often harmonic) or a two-state system. The system is typically coupled to a parametrized, fast-decaying bath. If multiple system coordinates are needed, they are generally uncorrelated and each coupled to a separate bath. Yet optical experiments often induce motion in multiple, coupled coordinates that interact with the same solvent molecules. This paper is a first step toward simulating the relaxation of more complicated models. While we too assume a parametrized, fast-decaying bath, our model system has three coupled,

anharmonic coordinates, and we explore several different forms of coupling to the bath.

Some relaxation phenomena can only occur with multiple system coordinates. Most simply, when different modes relax at different rates, the optical signal can be smoothed quickly but show only slow decay of the amplitude of a remaining oscillation. Widely different relaxation rates are most likely for system coordinates that are coupled to the same (or to correlated) bath modes; the combined influence can augment or shut off relaxation pathways. Thus, if multiple system coordinates in a normal mode drive the same bath mode in opposite directions, little energy will dissipate into that bath mode. Similar interference could occur in reverse if multiple bath coordinates are coupled to a single system mode; it would be manifested in larger or smaller correlation functions and values of $(\theta^{+}_{ab})_{\omega}$. As noted earlier, these effects are material analogues to super- and subradiance. When the system modes are coupled to each other, another phenomenon can occur; transfer between modes can depopulate states excited in one mode and slow relaxation in another mode. But this process was less important in our model system.

Our results also confirm the importance of processes other than simple dephasing and population relaxation, including "nonsecular" (oscillating) processes. Although individual Redfield tensor elements are useful for comparing different coupling forms, they are often very different from the actual energy dissipation and signal damping rates, especially due to "cascading" populations and transfer of coherence. The system energy often shows prominent oscillations due to coupling between populations and coherences. These couplings also affect the optical signal somewhat.

The time-resolved fluorescence Stokes shift is a specific probe of some types of relaxation. It is sensitive primarily to coherent motion of the system and is damped by dephasing. In contrast, energy dissipation, for which the Stokes shift is sometimes misconstrued to be an experimental measure, is due to population relaxation. In our model system at room temperature, population relaxation is mostly incoherent emission unrelated to system coherence. Thus, depending on the system−bath coupling form and the consequent relaxation rates, the signal can continue to oscillate when there is little superthermal energy left in the system or can be damped long before dissipation is complete. The fluorescence dynamics from an anharmonic system is damped by a variety of system−bath couplings, but the form of the coupling can affect the overall damping rate, the relative rate of damping of oscillations at different frequencies, and other details of the signal. This sensitivity likely would be washed out in typical overdamped solvation Stokes shift measurements, allowing simulation by a variety of coupling forms that may or may not correspond to the real system (although weak coupling approaches may not relax the system fast enough). But the difference between dissipation and coherence loss could be significant even in an overdamped system.

Our results have relevance for other approaches that have been used to simulate the relaxation of multimode systems. In particular, the multimode Brownian oscillator has been successfully applied to fit a variety of optical signals.[34−38] In this model, one or more displaced harmonic oscillators are each coupled to an independent bath. Usually the system and bath are both phenomenological (parametrized) and cannot easily be associated with specific molecular motions. For the specific case of a single displaced harmonic mode linearly coupled to an instantaneously relaxing bath, with adiabatic evolution, the Brownian oscillator model has been shown to be equivalent to Redfield relaxation.[32]

The assumption of independent relaxation of each system mode is somewhat different in general from our "uncorrelated" coupling case, in which the relaxation of each *local* system coordinate is independent. It is not clear why collective system modes made up of different motions of the same system atoms should be coupled to entirely independent bath modes. Uncorrelated relaxation of localized coordinates seems more plausible. Independent modes do not allow the transfer of energy between modes, which could be significant in anharmonic systems. However, independent modes with individually chosen relaxation rates could incorporate some of the interference effects described in section III.B.

The combination of harmonic system modes with linear coupling neglects pure dephasing. Such an approximation is particularly severe in simulating an optical signal such as fluorescence that is strongly affected by dephasing. Displaced harmonic modes without Duschinsky rotation or frequency changes also result in the wrong initial density matrix in the excited electronic state; if the model is based on the ground electronic state, the frequencies of motion could be wrong as well (note the different frequencies in the two states in our model system). On the other hand, the assumption of displaced harmonic modes in the multimode Brownian oscillator model allows strong coupling to a bath and hence enables simulation of overdamped modes. The limitations of the model may be less important in treating overdamped modes because of the lack of information in the fast-decaying dynamics.

For more slowly damped systems another method appears possible, if not easy. A few collective coordinates coupled to the electronic state and to each other could be picked out of the model of a solution to form the subsystem.[17] The system−bath coupling would be known from the full potential. The bath correlation functions could be estimated from classical simulation. This approach would allow simulation of a real solution (as real as the potential surface) instead of a set of parameters describing relaxation,[39] but it also would be restricted by the actual potential. Convenient assumptions such as weak coupling and Markovian separation of time scales would have to be justified or avoided rather than built in. How large the system would have to be to enable these approximations for the rest of a realistic bath remains an open question.

Acknowledgment. The authors thank Eric Hiller, Alex Matro, Tim Smith, and Howard Carmichael for helpful conversations. This research was supported by NSF Grant CHE-9546215 and by the Camille and Henry Dreyfus Teacher-Scholar Award Program.

References and Notes

(1) Redfield, A. G. *Adv. Magn. Reson.* **1965**, *1*, 1.

(2) Blum, K. *Density Matrix Theory and Applications*, 2nd ed.; Plenum: New York, 1996.

(3) Zadoyan, R.; Almy, J.; Apkarian, V. A. *J. Chem. Soc.−Faraday Discuss.* **1998**, *108*, 255. Zadoyan, R.; Sterling, M.; Apkarian, V. A. *J. Chem. Soc., Faraday Trans.* **1996**, *92*, 1821. Li, Z.; Zadoyan, R.; Apkarian, V. A.; Martens, C. C. *J. Phys. Chem.* **1995**, *99*, 7453.

(4) Silbey, R.; Harris, R. A. *J. Phys. Chem.* **1989**, *93*, 7062.

(5) Leggett, A. J.; Chakravarty, S.; Dorsey, A. T.; Fisher, M. P. A.; Garg, A.; Zwerger, W. *Rev. Mod. Phys.* **1987**, *59*, 1.

(6) Aslangul, C.; Pottier, N.; Saint-James, D. *J. Phys. (Paris)* **1986**, *47*, 1657.

(7) Makarov, D. E.; Makri, N. *Phys. Rev. A* **1993**, *48*, 3626. Makri, N. *J. Math. Phys.* **1995**, *36*, 2430.

(8) Cao, J.; Voth, G. A. *J. Chem. Phys.* **1994**, *100*, 5106; **1994**, *101*, 6157; **1994**, *101*, 6168.

(9) Georgievskii, Y.; Hsu, C.-P.; Marcus, R. A. *J. Chem. Phys.* **1998**, *108*, 7356.
(10) Tully, J. C. *J. Chem. Phys.* **1990**, *93*, 1061.
(11) Webster, F.; Rossky, P. J.; Friesner, R. A. *Comput. Phys. Commun.* **1991**, *63*, 494.
(12) Bittner, E. R.; Rossky, P. J. *J. Chem. Phys.* **1995**, *103*, 8130.
(13) Ungar, L. W.; Cina, J. A. *Adv. Chem. Phys.* **1997**, *100*, 171.
(14) For classical simulations of bulk polar solvation dynamics see: Maroncelli, M. *J. Mol. Liq.* **1993**, *57*, 1. Ladanyi, B. M.; Stratt, R. M. *J. Phys. Chem.* **1995**, *99*, 2502.
(15) Cao, J. *J. Chem. Phys.* **1997**, *107*, 3204.
(16) Oxtoby, D. *Adv. Chem. Phys.* **1979**, *40*, 1; *Adv. Chem. Phys.* **1981**, *47*, 487.
(17) Pollard, W. T.; Friesner, R. A. *J. Chem. Phys.* **1994**, *100*, 5054. Pollard, W. T.; Felts, A. K.; Friesner, R. A. *Adv. Chem. Phys.* **1996**, *93*, 77.
(18) Equations of motion similar though not identical in form to eq 5—but involving only $N \times N$ matrix multiplication and conferring the same computational advantage—are used in quantum optics; see, for example: Louisell, W. H. *Quantum Statistical Properties of Radiation*; John-Wiley and Sons: New York, 1973; section II.
(19) Matro, A.; Cina, J. A. *J. Phys. Chem.* **1995**, *99*, 2568.
(20) Gai, H.; Voth, G. A. *J. Chem. Phys.* **1993**, *99*, 740. Sun, Y.-C.; Gai, H.; Voth, G. A. *Chem. Phys.* **1996**, *205*, 11.
(21) See, however, Bader, J. S.; Berne, B. J. *J. Chem. Phys.* **1994**, *100*, 8359. Skinner, J. L. *J. Chem. Phys.* **1997**, *107*, 8717.
(22) Ungar, L. W.; Scherer, N. F. Manuscript in preparation.
(23) Jean, J. M.; Friesner, R. A.; Fleming, G. R. *J. Chem. Phys.* **1992**, *96*, 5827. Jean, J. M. *J. Chem. Phys.* **1994**, *101*, 10464. Jean, J. M.; Fleming, G. R. *J. Chem. Phys.* **1995**, *103*, 2092. Jean, J. M. *J. Chem. Phys.* **1996**, *104*, 5638. Jean, J. M. *J. Phys. Chem.*, submitted.
(24) Landau, L. D.; Lifshitz, E. M. *Statistical Physics*, 3rd ed.; Pergamon: New York, 1980; Part 1. The equations used in the text are eqs 123.11 and 126.1.
(25) The recent work by Georgievskii, Hsu, and Marcus (ref 9) considers the time-dependent transition energy following a noninstantaneous excitation pulse, but without explicit treatment of the upconversion pulse, for a quantum multidimensional displaced harmonic oscillator system. Another recent paper gives formal expressions for the doorway and window operators appropriate to spontaneous light emission experiments in the absence of temporal pulse overlap. Mukamel, S.; Ciordas-Ciurdariu, C.; Khidekel, V. *Adv. Chem. Phys.* **1997**, *101*, 345.
(26) Proper incorporation of system−bath interaction during overlapping and nonoverlapping pulses will be addressed in forthcoming work by Shen, Y. C.; Cina, J. A., 1998.
(27) Press, W. H.; Flannery, B. P.; Teukolsky, S. A.; Vetterling, W. T. *Numerical Recipes*; Cambridge University Press: Cambridge, 1986.
(28) Maroncelli, M. *J. Chem. Phys.* **1991**, *94*, 2084.
(29) Edwards, D. M. F.; Madden, P. A.; McDonald, I. R. *Mol. Phys.* **1984**, *51*, 1141.
(30) Zadoyan, R.; Sterling, M.; Ovchinnikov, M.; Apkarian, V. A. *J. Chem.. Phys.* **1997**, *107*, 8446.
(31) Dicke, R. H. *Phys. Rev.* **1954**, *93*, 99.
(32) Kohen, D.; Tannor, D. J. *J. Chem.. Phys.* **1997**, *107*, 5141. Kohen, D.; Marston, C. C.; Tannor, D. J. *J. Chem. Phys.* **1997**, *107*, 5236.
(33) The initial superthermal energy is slightly lower at room temperature because the excitation pulse is resonant with the center of the initial population distribution, where the low-energy components of the distribution are concentrated. The initial superthermal energy can be simply expressed for the case of one-dimensional displaced harmonic potentials. Under the classical Franck approximation, eqs 3.13−3.15 and 3.19 of ref 13 give the initial moments of the nuclear distribution in the excited electronic state in terms of the moments at thermal equilibrium. From those moments one can obtain

$$\langle H_e\rangle_g - \langle H_e\rangle_e = (\tau_p\Delta)^2\left(\frac{1}{4m} - \frac{m\,\omega^2}{\hbar^2}\langle x^2\rangle_e^2\right) + \frac{m\omega^2}{2}x_e^2 = \frac{m\,\omega^2}{2}x_e^2\left[1 - \frac{(\omega\tau_p)^2}{2\sinh^2(\hbar\beta\omega/2)}\right]$$

where τ_p is the excitation pulse duration, $\Delta = -m\omega^2 x_e$ is the slope of the difference potential, x_e is the excited-state displacement, and $\langle x^2\rangle_e = \hbar/2m\omega\,\coth(\hbar\beta\omega/2)$ is the equilibrium second moment of the coordinate. $\langle x^2\rangle_e$ increases and the initial superthermal energy decreases with increasing temperature.
(34) Yan, Y. J.; Mukamel, S. *J. Chem. Phys.* **1988**, *89*, 5160. Tanimura, Y.; Mukamel, S. *Phys. Rev. E* **1993**, *47*, 118. Mukamel, S. *Principles of Nonlinear Optical Spectroscopy*; Oxford University Press: New York, 1995.
(35) Nibbering, E. T. J.; Duppen, K.; Wiersma, D. A. *J. Photochem. Photobiol., A* **1992**, *62*, 347.
(36) Vöhringer, P.; Arnett, D. C.; Westervelt, R. A.; Feldstein, M. J.; Scherer, N. F. *J. Chem. Phys.* **1995**, *102*, 4027.
(37) Fried, L. E.; Bernstein, N.; Mukamel, S. *Phys. Rev. Lett.* **1992**, *68*, 1842. Fried, L. E.; Mukamel, S. *Adv. Chem. Phys.* **1993**, *84*, 435.
(38) de Boeij, W. P. *Ultrafast Solvation Dynamics Explored by Nonlinear Optical Spectroscopy*; Proefschrift: Rijksuniversiteit Gröningen, 1997.
(39) It will be interesting in this case to entertain the possible existence of resonant couplings, bifurcations, and nonlinear normal modes comprising both chromophore and solvent degrees of freedom. For an introduction to these structures in polyatomic molecules, see: Kellman, M. E. *Annu. Rev. Phys. Chem.* **1995**, *46*, 395.